Comparison of Second-Order Loads on a Tension-Leg Platform for Wind Turbines

Preprint

S. Gueydon
Maritime Research Institute of The Netherlands (MARIN)

P. Wuillaume
MARIN Academy

J. Jonkman, A. Robertson, and A. Platt
National Renewable Energy Laboratory

To be presented at the Twenty-Fifth International Offshore and Polar Engineering Conference
Kona, Hawaii
June 21–26, 2015

NREL is a national laboratory of the U.S. Department of Energy
Office of Energy Efficiency & Renewable Energy
Operated by the Alliance for Sustainable Energy, LLC

This report is available at no cost from the National Renewable Energy Laboratory (NREL) at www.nrel.gov/publications.

Conference Paper
NREL/CP-5000-63840
March 2015

Contract No. DE-AC36-08GO28308

This report is available at no cost from the National Renewable Energy Laboratory (NREL) at www.nrel.gov/publications.

Available electronically at http://www.osti.gov/scitech

Available for a processing fee to U.S. Department of Energy and its contractors, in paper, from:

U.S. Department of Energy
Office of Scientific and Technical Information
P.O. Box 62
Oak Ridge, TN 37831-0062
phone: 865.576.8401
fax: 865.576.5728
email: mailto:reports@adonis.osti.gov

Available for sale to the public, in paper, from:

U.S. Department of Commerce
National Technical Information Service
5285 Port Royal Road
Springfield, VA 22161
phone: 800.553.6847
fax: 703.605.6900
email: orders@ntis.fedworld.gov
online ordering: http://www.ntis.gov/help/ordermethods.aspx

Cover Photos: (left to right) photo by Pat Corkery, NREL 16416, photo from SunEdison, NREL 17423, photo by Pat Corkery, NREL 16560, photo by Dennis Schroeder, NREL 17613, photo by Dean Armstrong, NREL 17436, photo by Pat Corkery, NREL 17721.

NREL prints on paper that contains recycled content.

Comparison of Second-Order Loads on a Tension-Leg Platform for Wind Turbines

Sébastien Gueydon[1], Pierre-Yves Wuillaume[2], Jason Jonkman[3], Amy Robertson[3], Andrew Platt[3]

[1]Maritime Research Institute of The Netherlands (MARIN)
Wageningen, The Netherlands

[2]MARIN Academy
Wageningen, The Netherlands

[3]National Renewable Energy Laboratory (NREL)
Golden, Colorado, USA

ABSTRACT

The first objective of this work is to compare the two floating offshore wind turbine simulation packages; (DIFFRAC+aNySIM) and (WAMIT+FAST). The focus of this study is on second-order wave loads; therefore, first- and second-order wave loads are applied to a structure sequentially for a detailed comparison and a more precise analysis of the effects of the second-order loads. aNySIM does not have the capability to model flexible bodies, so the simulations performed in this tool are done assuming a rigid body. FAST also assumes that the platform is rigid but can account for the flexibility of the tower. The second objective is to study the effects of the second-order loads on the response of a tension-leg platform (TLP) floating wind turbine. The flexibility of the tower must be considered for this investigation; therefore, only FAST is used.

KEY WORDS: Tension-leg platform; TLP; second-order; resonance; sum-frequency; diff-frequency; flexibility; FAST; aNySIM; WAMIT; DIFFRAC.

NOMENCLATURE

A	hydrodynamic added mass matrix	kg, kg.m, kg.m^2
B	hydrodynamic damping matrix	N.s/m, N.s, N.m.s
C	hydrostatic stiffness matrix	N/m, N, N.m
dl	element of the water line contour	m
dS	surface element of the wetted hull	m^2
$F_{(1)}$	first-order wave forces	N, N.m
$F_{(2)}$	second-order wave forces	N, N.m
g	gravity constant	m/s^2
K	mooring stiffness matrix	N/m, N, N.m
M	mass matrix of the body	kg, kg.m, kg.m^2
n_0	outward pointing normal vector	-
N	number of wave harmonics	-
O	origin of the underwater geometry at swl	
P	In-phase part of the quadratic transfer function	N/m^2, N.m/m^2
Q	Out-phase part of the quadratic transfer function	N/m^2, N.m/m^2
S	wetted surface of the hull	m^2
swl	still water line	
t	time	s
W.L.	*W*ater *L*ine	
X	6 component vector with positions of point O	
$X(1)$	surge	m
$X(2)$	sway	m
$X(3)$	heave	m
$X(4)$	roll	rad
$X(5)$	pitch	rad
$X(6)$	yaw	rad
$\ddot{X}$	second time derivative of vector X	m/s^2, rad/s^2
ε_j	random phase of j^{th} wave harmonic	rad
ζ_j	amplitude of j^{th} wave harmonic	m
ζ_{rel}	relative wave elevation	m
ϕ	velocity potential	m^2/s
Ω	angular motion vector	rad
ω_j	j^{th} wave frequency	rad/s
ρ	mass density of water	kg/m^3

INTRODUCTION

Wind is a sustainable energy source that can be harvested on a large scale to supply clean electricity at a competitive price. In some coastal areas with a high electricity demand and no shallow water, floating platforms are a promising solution for offshore wind turbines. The design of floating offshore wind turbines requires sophisticated numerical tools that capture the coupled aerodynamics, hydrodynamics, control and electrical-drive dynamics, and structural dynamics of the full system nonlinearly in the time domain. The inherent sophistication of these tools warrants model-to-model verification at the module and integrated levels.

In previous work (Gueydon et al, 2014), we verified the hydrodynamic wave-body interaction with first- and second-order potential-flow solutions for a semisubmersible by comparing two tools—FAST (Jonkman and Buhl, 2005), developed by the National Renewable Energy Laboratory (NREL), and aNySIM (online User Guide), developed by Maritime Research Institute Netherlands (MARIN). In that work, WAMIT, developed by WAMIT, Inc. (Lee, 2013), and DIFFRAC, developed by MARIN (Bunnik, 2012), were used to

generate the first- and second-order potential-flow hydrodynamic radiation and diffraction solutions in the frequency domain using the boundary element method (BEM). The solutions are transformed to the time domain within FAST and aNySIM, respectively. While first-order potential-flow solutions have been studied in many projects (Jonkman et al, 2010; Robertson et al, 2012), the second-order solutions have not been widely studied. However, the magnitude and frequency content of second-order hydrodynamic loads can excite structural natural frequencies, leading to greater ultimate and fatigue loads than can be predicted solely using first-order theory. The previous work showed good overall agreement between FAST+WAMIT and aNySIM+DIFFRAC; however, while the second-order difference-frequency loads were shown to introduce slow-drift motions, the second-order sum-frequency effects were negligible in the semisubmersible studied.

In this work, a similar verification project is undertaken, but using a tension-leg platform (TLP), which due to its stiff tendons, has been known to be strongly affected by second-order sum-frequency effects. Therefore., second-order difference-frequency loads are expected to excite surge and sway modes, and second-order sum-frequency loads are expected to excite heave, roll, and pitch modes. The objectives of this project are to compare the solutions of FAST+WAMIT and aNySIM+DIFFRAC, with a focus on second-order effects, and to study the effects of second-order loads on the system response. In comparison to other kinds of floaters (such as a spar or a semisubmersible), the TLP has several notable advantages: its vertical motions are negligible, its weight is lighter, and its mooring system's footprint is smaller.

While first-order radiation and diffraction effects are uncoupled and depend only on geometry, the second-order solution is inherently coupled, depending not only on geometry, but also on the first-order motions that depend on the mass, damping, and stiffness of the station-keeping system and supported wind turbine. Unlike a spar or semisubmersible, the first-order motions of a TLP are strongly affected by the bending of the tower, which connects the floater with the rotor-nacelle assembly (Molin et al, 2004; Matha, 2009). Although it is not possible to model tower flexibility using BEM tools such as WAMIT and DIFFRAC, a workaround was employed in this paper to characterize the effect.

SECOND-ORDER WAVE LOADS

According to Pinkster (1980), second-order wave forces can be written as the summation of five different components when they are determined by direct pressure integration:

$$\begin{aligned}\overrightarrow{F_{(2)}} = & \\ & -\frac{1}{2}\rho g \int_{WL} \zeta_{(1),rel}^2 . \overrightarrow{n_0} . \overrightarrow{dl} && \text{I} \\ + & \frac{1}{2}\rho \iint_S \nabla\phi_{(1)} \cdot \nabla\phi_{(1)} . \overrightarrow{n_0}\, dS && \text{II} \\ + & \iint_S \rho . X_{(1)} \cdot \nabla \frac{\partial \phi_{(1)}}{\partial t} . \overrightarrow{n_0} dS && \text{III} \\ + & \vec{\Omega}_{(1)} \times M . \ddot{\vec{X}}_{(1)} && \text{IV} \\ - & \iint_S -\rho \cdot \nabla \frac{\partial \phi_{(2)}}{\partial t} . \overrightarrow{n_0} dS && \text{V}\end{aligned} \quad (1)$$

Subscript $_{(1)}$ denotes when a quantity is of the first order and $_{(2)}$ denotes when a quantity is of the second order.

Because components I to IV are quadratic contributions of the first-order solution, they can be fully determined from the first-order solution. The fifth component involves the second-order velocity potential that can be calculated by a second-order diffraction code applying the perturbation method. It is noted that DIFFRAC and WAMIT do not determine this component in the same way. In DIFFRAC, the component V is approximated. Only the contribution of the undisturbed incoming wave to the wave-exciting force is kept at the second order for the high-frequency component. In WAMIT, the second-order velocity potential includes the contribution of the undisturbed incoming wave, as well as the contributions of the diffracted and radiated waves.

The second-order force can be split into a low-frequency component $F_{(2),D}$ and a high-frequency component $F_{(2),S}$ (Eq. 2). Each component can be written with a double summation (Eq. 3 and 4). In Eq. 3, P_{ij}^- and Q_{ij}^- are respectively the in-phase and out-phase parts of the difference-frequency quadratic transfer function (QTF). P_{ij}^+ and Q_{ij}^+ are respectively the in-phase and out-phase sum-frequency components of the QTF (Eq. 4). The QTFs shown in this paper are made dimensionless according to the definition of WAMIT's chapter 11 (Lee, 2013).

$$F_{(2)} = F_{(2),D} + F_{(2),S} \quad (2)$$

$$\begin{aligned}F_{(2),D} = & \sum_{i=1}^{N}\sum_{j=1}^{N} \zeta_{(1),i}\zeta_{(1),j} P_{ij}^- \cos[(\omega_i - \omega_j)t + (\varepsilon_i - \varepsilon_j)] \\ & + \sum_{i=1}^{N}\sum_{j=1}^{N} \zeta_{(1),i}\zeta_{(1),j} Q_{ij}^- \sin[(\omega_i - \omega_j)t + (\varepsilon_i - \varepsilon_j)]\end{aligned} \quad (3)$$

$$\begin{aligned}F_{(2),S} = & \sum_{i=1}^{N}\sum_{j=1}^{N} \zeta_{(1),i}\zeta_{(1),j} P_{ij}^+ \cos[(\omega_i + \omega_j)t + (\varepsilon_i + \varepsilon_j)] \\ & + \sum_{i=1}^{N}\sum_{j=1}^{N} \zeta_{(1),i}\zeta_{(1),j} Q_{ij}^+ \sin[(\omega_i + \omega_j)t + (\varepsilon_i + \varepsilon_j)]\end{aligned} \quad (4)$$

TLP MODEL

TLP Description

In 2011, the DeepCwind consortium tested three different types of floating support platforms for a horizontal-axis wind turbine: a spar, a TLP, and a semisubmersible. All three floaters had the same turbine on top and were tested in the offshore basin of MARIN using both wind and wave excitation. The present study examined the behavior of the TLP in waves using numerical simulations. The TLP (Fig. 1) was only placed in long crested head waves. There was no wind and the turbine was parked. This platform was moored in 200-m water depth by three tendons with an equal pretension of 4,837 kilonewtons (kN). The mooring system is modeled as a spring. Table 1 gives the most relevant characteristic data for the work presented in this paper. However, more details can be found in other technical publications (Goupee et al, 2012, Prowell et al, 2013). Note that the floater's characteristics, its response, and the wave loads are all represented at full scale in this paper, whereas the actual model tests were done at 1/50 scale.

Fig. 1: Photo of the TLP in the basin

Table 1. Characteristics of the moored TLP with the turbine on top as built for the model tests of 2011.

	Units	Values
Mass	kg	1361E3
Displacement	m^3	2770.7
Draft	m	30.0
Centre of gravity above keel	m	64.06
Pitch radius of inertia	m	52.69
Angle between each pontoon	deg	120
Pre-tension	N	4837E3
Tendon axial stiffness	N	8.29E9

Numerical Model of The Rigid TLP

A potential-flow (PF) model of the TLP was made. The same mesh of the immersed part of the TLP is used for both PF numerical tools (Fig. 2):

- DIFFRAC of MARIN
- WAMIT of WAMIT Inc.

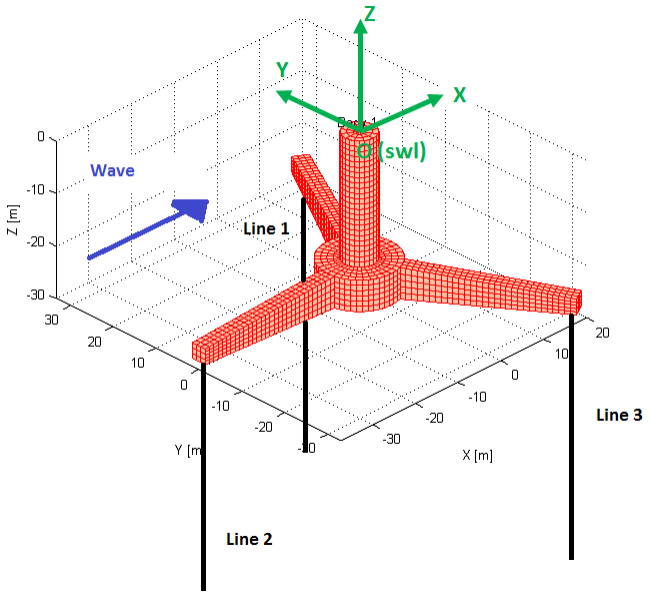

Fig. 2: Geometry of the TLP and conventions

From this model, the geometry is used to determine the coefficients for the added-mass, the potential damping, and the linear wave-excitation loads. Several meshes with an increasing number of panels were used to ensure that the first-order solution had converged. The resulting coefficients are plotted in Fig. 3, 4, and 5. All results in this paper are given at the point O of Fig. 2, which is located at the midship, center, and still water level (swl). As the waves travel in the direction of the surge axis of Fig 2 (+x) and the rotor is not spinning, only quantities related to the surge and heave translations and the pitch rotation are presented.

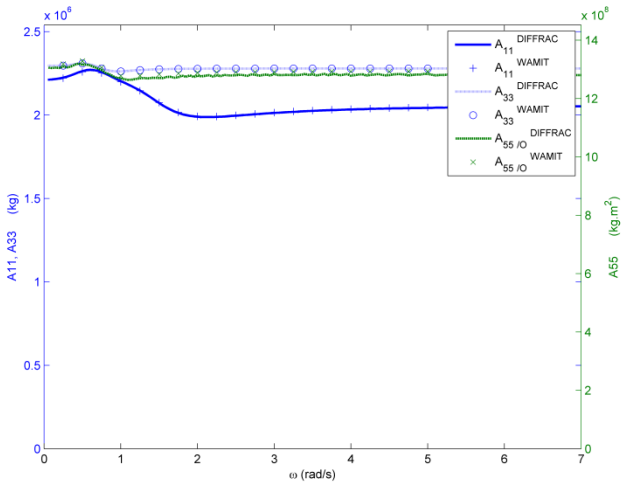

Fig. 3: Added-mass coefficients

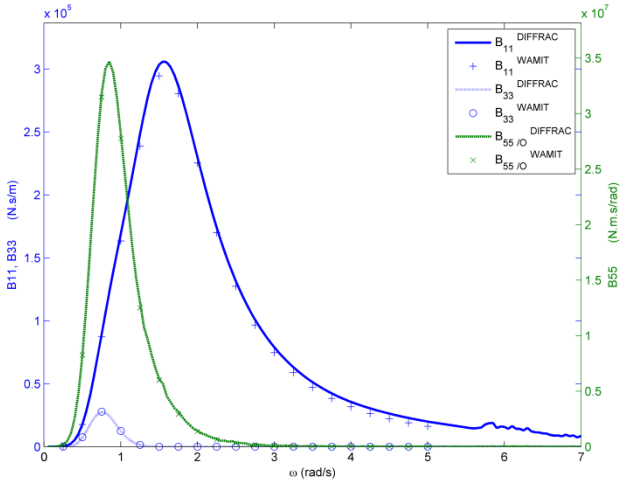

Fig. 4: Potential damping coefficients

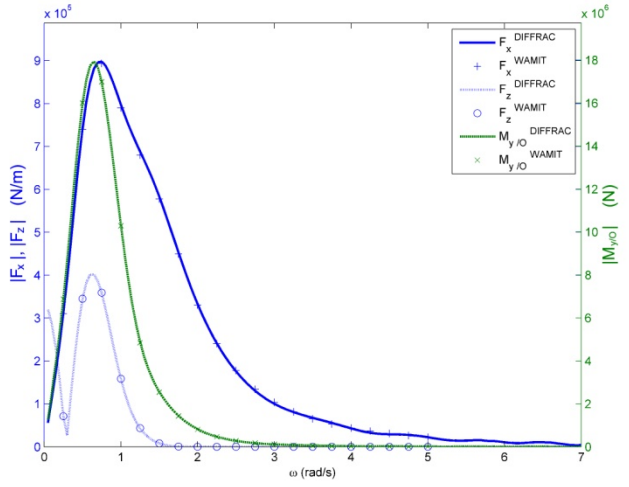

Fig. 5: Amplitude of first-order wave-excitation load transfer functions

Prior to the calculation of the second-order solution, the first-order motion responses must be determined. This is done by solving the systems' equations of motion in the frequency domain. At this stage, the full inertia of the system and the total combined stiffness from hydrostatics and moorings must be known—see Table 2. The equivalent stiffness matrix was determined for the mooring system through simple algebra (Wuillaume, 2014).

Table 2. Spring characteristics.

	Symbol	Units	Values
Hydrostatic stiffness along z-axis	C_{33}	N/m	3.33E5
Hydrostatic stiffness around y-axis	$C_{55/O}$	N.m/rad	-6.31E8
Mooring stiffness along x-axis	K_{11}	N/m	8.46E4
Mooring stiffness along z-axis	K_{33}	N/m	1.45E8
Mooring stiffness around y-axis	$K_{55/O}$	N.m/rad	6.54E10

When modeled as a rigid body, the eigenmodes of the TLP can be determined from these mass and stiffness terms and the linear solution of the potential-flow problem. Table 3 contains the frequencies of the main rigid-body modes. In addition to the radiation contribution of the potential-flow theory to the damping, viscous loads are added to the hydrodynamic loading. The viscous effects are introduced in the model by additional linear damping coefficients. The role of this additional damping is to limit the amplitude of the resonance peaks occurring at the frequencies given in Table 3. Therefore, the additional damping is expressed as a percentage of the critical damping for each mode.

Table 3. Eigenfrequencies of the whole system seen as a rigid body.

Eigen modes & viscous damping	Symbol	rad/s	% of critical damping
Translation along x-axis (Surge)	ω_1	0.15	2.5
Translation along z-axis (Heave)	ω_3	6.3	2.5
Rotation around y-axis (Pitch)	ω_5	3.1	2.7

Knowing where resonance may happen, a suitable range of frequencies can be chosen for the second-order wave loading. Hence, the difference-frequency QTF is determined using first-order results for a frequency range of [0.05; 1.6] rad/s where there is wave energy. The bandwidth of the QTF is chosen so that it largely contains the surge eigenfrequency (Fig. 6). The two black dotted lines plotted on Fig. 6 show the difference frequency equal to the surge eigenfrequency. The sum-frequency QTF is calculated based on first-order results from [0.3; 3.5] (rad/s) so that the sum-frequencies include the pitch and the heave eigenfrequencies. The sum frequency equal to the pitch eigenfrequency of the rigid TLP is drawn on Fig. 7 with a black dotted line.

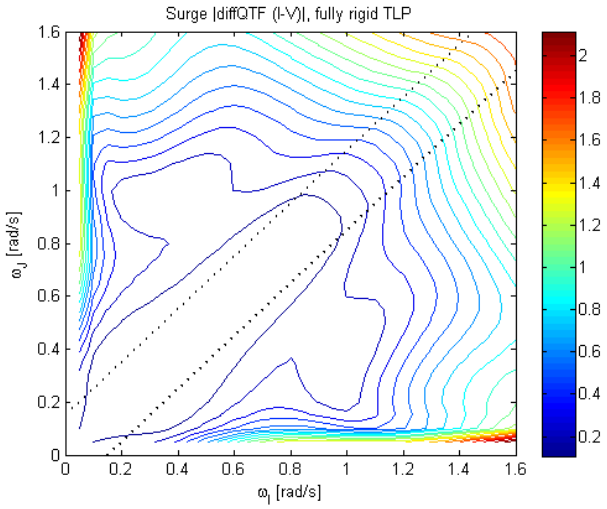

Fig. 6: Amplitude of surge difference-frequency QTF for the rigid TLP (the dotted lines correspond to difference frequencies of $\pm\omega_1$, the surge eigenfrequency).

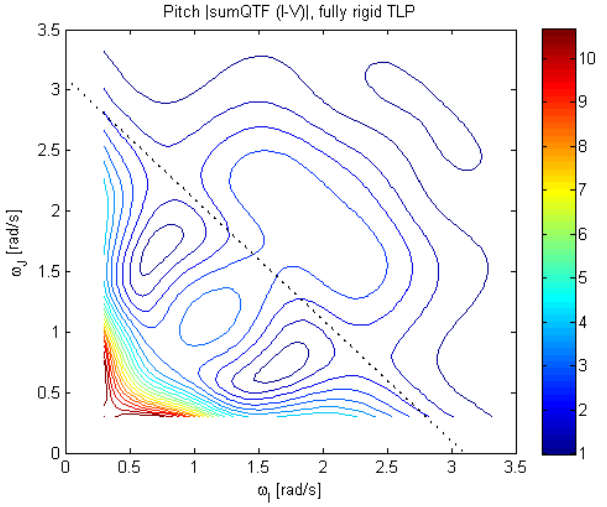

Fig. 7: Amplitude of pitch sum-frequency QTF for the rigid TLP (the dotted line corresponds to sum frequencies of ω_5, the pitch eigenfrequency for the fully rigid TLP).

Numerical Model of The Flexible TLP

During the MARIN experiments, we observed that the pitch eigenfrequency was lower than the value in Table 3. This can be explained by the effect of the flexibility of the model. Molin et al (2004) and Matha (2009) showed that the flexibility of the tower is the main cause of the decrease of the pitch eigenfrequency, as this mode is coupled with the first tower-bending mode. Using FAST, the flexibility of the tower can be accounted for by including 6 degrees of freedom (DOFs) for the motion of the TLP foundation, plus additional DOFs to represent the deformation modes of the tower (one extra per bending mode). Table 4 gives the eigenmodes that FAST calculated. In this way, the response of the TLP with a flexible tower can be simulated by FAST.

As seen before, using the correct first-order motion response is also important to determine the second-order excitation loads. Thus, the pitch response, which is affected by the elasticity of the tower, cannot

be ignored for the calculation of the second-order loads. However, the number of DOFs for the TLP foundation is fixed to 6 for a single rigid body in DIFFRAC and WAMIT. As a consequence, there is no direct way to include the effect of the tower's flexibility in the hydrodynamic database of the TLP. A work-around for approximating the effect consists of substituting the pitch response of the rigid body by its pitch response with the flexible tower. In other words, the pitch resonance peak of the TLP can be shifted to the new frequency of the tower's first bending mode. In this approach, the total stiffness coefficient in pitch (C55+K55) is adjusted so that the resonance peak occurs at the eigenfrequency of the TLP with the flexible tower. Figure 8 shows how the new equivalent stiffness is determined. The upwards triangle marker corresponds to (C55+K55) of the rigid TLP (at 3.1 rad/s), and the downwards triangle marker gives the equivalent value of (C55+K55) for the TLP with the flexible tower (at 1.8 rad/s). The new value of the total stiffness in pitch (and roll) is 2.3E10 N.m/rad.

Acknowledging that only the pitch and roll are affected by the elasticity of the tower, the stiffness values for surge, sway, heave, and yaw stay equal to the values used for the rigid TLP. The first-order motion responses (Fig. 9) are then obtained with this new value for the stiffness in pitch (and roll), and these responses are used in the calculation of the second-order excitation loads. As a result, new QTFs are plotted (Figs. 10 and 11). The surge difference-frequency QTFs look almost identical whether the pitch response of the rigid or the flexible body is used. On the contrary, the sum-frequency QTF looks a bit different. The amplitudes of its peaks are slightly higher and their locations are different. More importantly, the lines corresponding to the sum frequency, which are equal to the pitch eigenfrequencies with or without the tower flexibility, cross the QTFs in very distinct sections.

Table 4. Eigenfrequencies of the moored TLP with the turbine on top, modeled as a flexible body.

Eigen frequency	Units	Values
Translation along x-axis (Surge)	rad/s	0.15
Translation along z-axis (Heave)	rad/s	6.3
Pitch/tower first bending mode	rad/s	1.8
Pitch/tower second bending mode	rad/s	>7.0

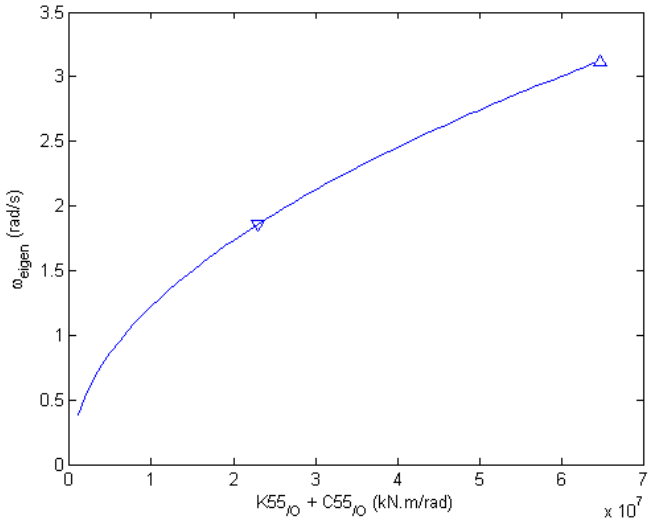

Fig. 8: Eigenfrequency in pitch as a function of the pitch stiffness

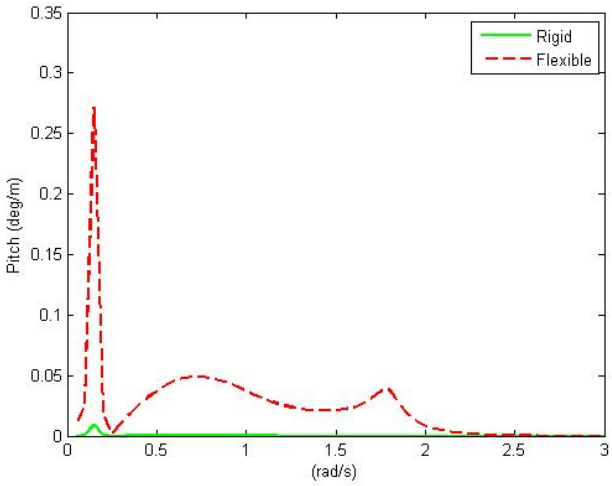

Fig. 9: Pitch responses used for the second-order calculation

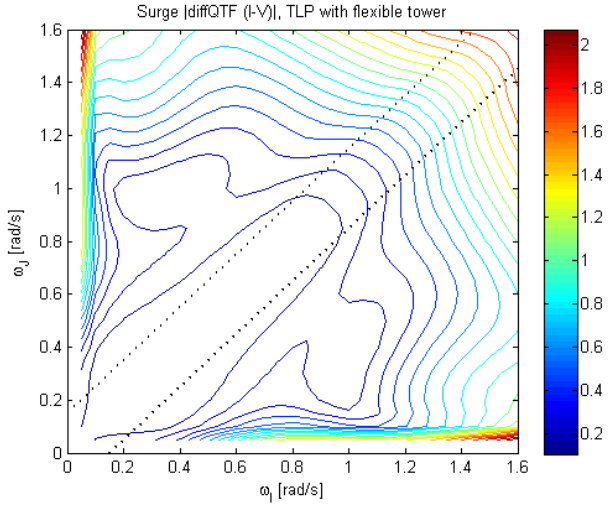

Fig. 10: Amplitude of surge difference-frequency QTF for the TLP with the flexible tower (the dotted lines correspond to difference frequencies of $\pm\omega_1$, the surge eigenfrequency).

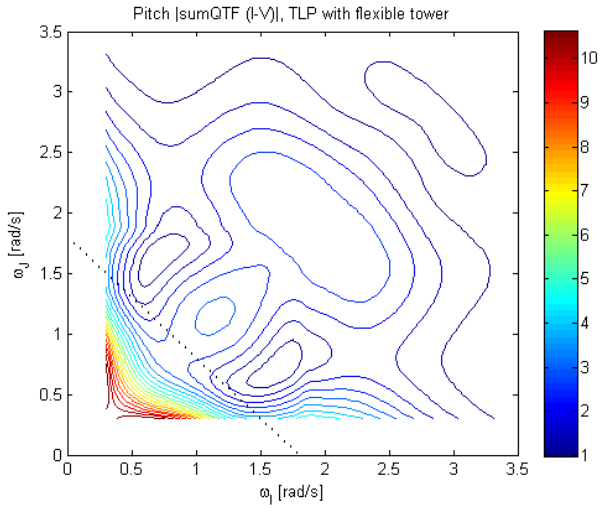

Fig. 11: Amplitude of pitch sum-frequency QTF for the TLP with the flexible tower (the dotted line corresponds to sum frequencies of ω_5, the pitch eigenfrequency for the TLP with the flexible tower).

RESULTS

Load Cases

This section describes the load cases applied to the rigid TLP in the comparison study.

Load case 2.2 (LC2.2) from Phase 2 of the Offshore Code Comparison Collaboration Continuation (OC4) benchmark study (Robertson, 2012) was chosen for the simulations. While OC4 Phase 2 LC2.2 was originally applied to a semisubmersible, it is applied in this paper to the TLP. In LC2.2, the floater is exposed to a mono-directional JONSWAP wave spectrum with a significant wave height of 6 m, a peak period of 10 s, and a peak enhancement factor of 2.87. A first-order cut-off frequency is set at 1.57 rad/s. The same wave train is used by aNySIM and FAST. Its power density spectrum (PSD) is plotted on the same graph as the theoretical spectrum in Fig. 12 (normally distributed amplitudes were used) together with a dotted line showing the wave cut-off frequency. To gain more insight into the results of both programs, LC2.2 is split into six cases in which the components of the wave loads are applied incrementally:

- LC2.2-F1: first-order wave loads only
- LC2.2-F1+F2D: first- and second-order difference-frequency loads
- LC2.2-F1+F2DQ: first- and second-order difference-frequency loads with only the sum of quadratic terms (components I + II + III + IV of Eq. 1)
- LC2.2-F1+F2S: first- and second-order sum-frequency loads
- LC2.2-F1+F2SQ: first- and second-order sum-frequency loads with only the sum of quadratic terms (components I + II + III + IV of Eq. 1)
- LC2.2-ALL: all components of first- and second-order loads together.

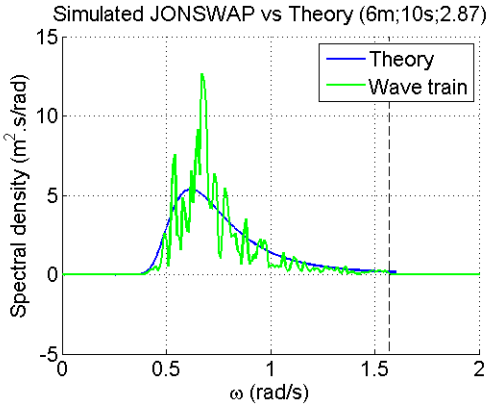

Fig. 12: Fourier Transformation of the wave train of LC2.2

Comparison Study for the Rigid TLP

The motion responses of the rigid TLP of (DIFFRAC+aNySIM) and (WAMIT+FAST) are compared. All motions are given at the location noted O in Fig. 2.

The first-order responses to the waves are checked through the comparison of response amplitude operators (RAOs). These RAOs are calculated for a frequency range where the wave energy is higher than 0.05% of its peak. RAOs for surge, heave, and pitch are calculated from the results of aNySIM and FAST for LC2.2-F1.These RAOs are plotted with those of the linear solution of the potential-flow problem (i.e. DIFFRAC and WAMIT). As can be seen in Figs 13,14, and 15, the comparison of the first-order results is excellent.

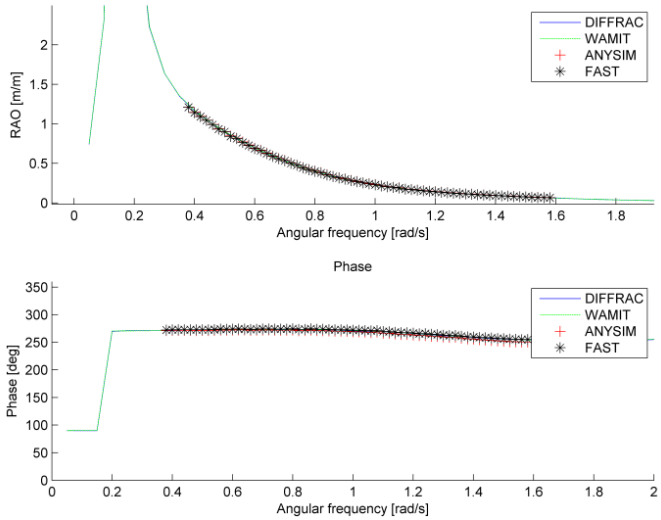

Fig. 13: Surge RAO for the fully rigid TLP

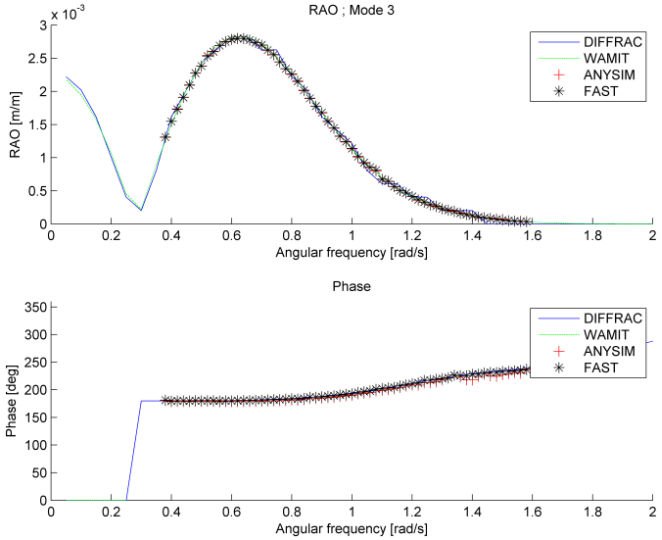

Fig. 14: Heave RAO for the fully rigid TLP

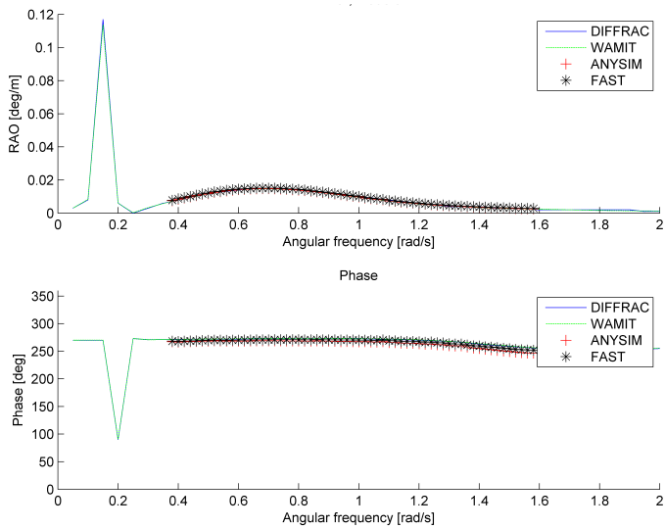

Fig. 15: Pitch RAO for the fully rigid TLP

In a second step, the second-order wave loads are added to the linear wave loads. The second-order loads are applied to the floater in aNySIM and FAST through double inverse Fourier transforms of the product of wave-amplitude pairs and the QTFs (Eq. 2 to 4). These QTFs are the result of the potential-flow problem extended to second order. The QTFs of DIFFRAC and WAMIT look very similar despite the modeling differences previously explained (Wuillaume, 2014). No remarkable differences can be seen between the results of (DIFFRAC+aNySIM) and (WAMIT+FAST) in Figs.16 and 17. Figure 18 shows the results of the simulations of LC2.2-ALL versus the results of LC2.2-F1. For the rigid body, the effects of the second-order loads are very small and mainly limited to the surge response. The difference-frequency second-order loads cause a small but visible variation of the surge motion, whereas no other noticeable variations are caused by the sum-frequency loads for the rigid TLP due to the very high natural frequencies (Table 3).

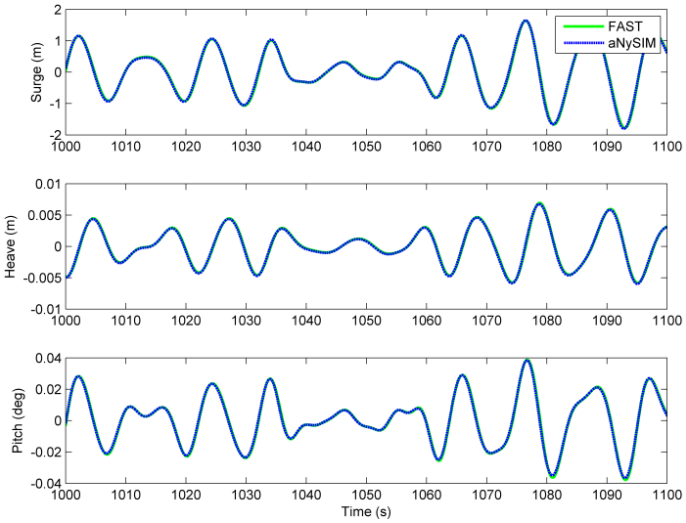

Fig. 16: Comparison of rigid TLP motions (DIFFRAC+aNySIM) and (WAMIT+FAST) for load case LC2.2-F1+F2S.

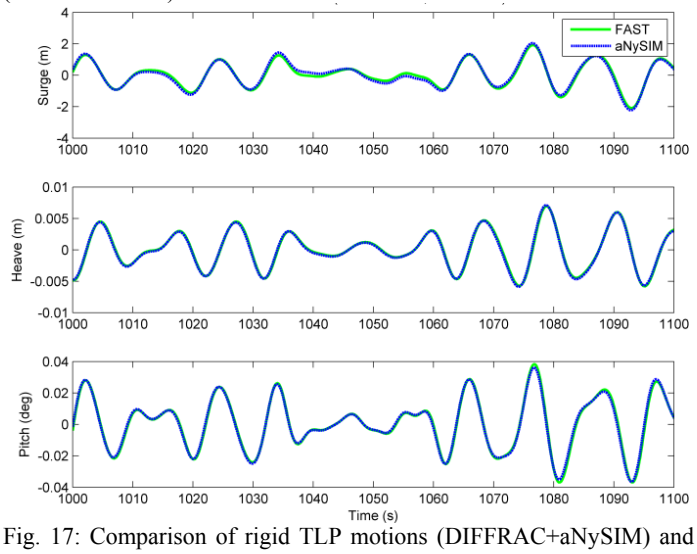

Fig. 17: Comparison of rigid TLP motions (DIFFRAC+aNySIM) and (WAMIT+FAST) for load case LC2.2-F1+F2D.

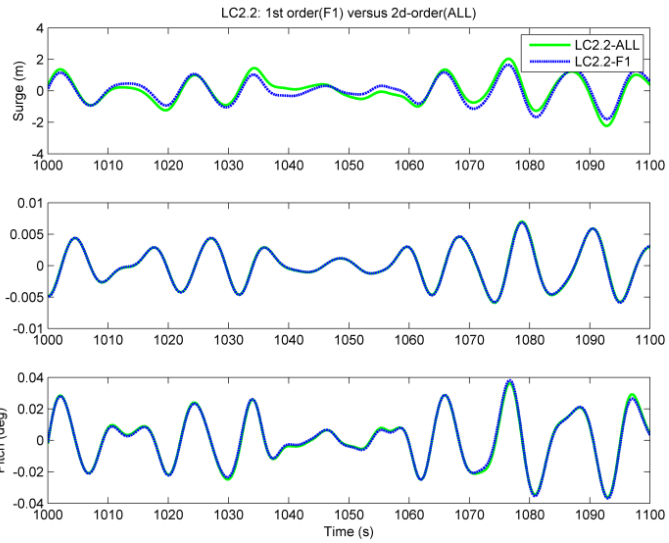

Fig. 18: Effects of second-order loads on motions in comparison to first-order simulations with aNySIM for the rigid TLP.

TLP with Flexible Tower

The motion responses of the TLP with a flexible tower are compared to those of a fully rigid system—see the FAST results in Fig. 19. We observed that the tower's flexibility affects only the pitch rotation. The pitch rotation is increased and is also subjected to more frequent variations with the flexible tower than with the rigid tower.

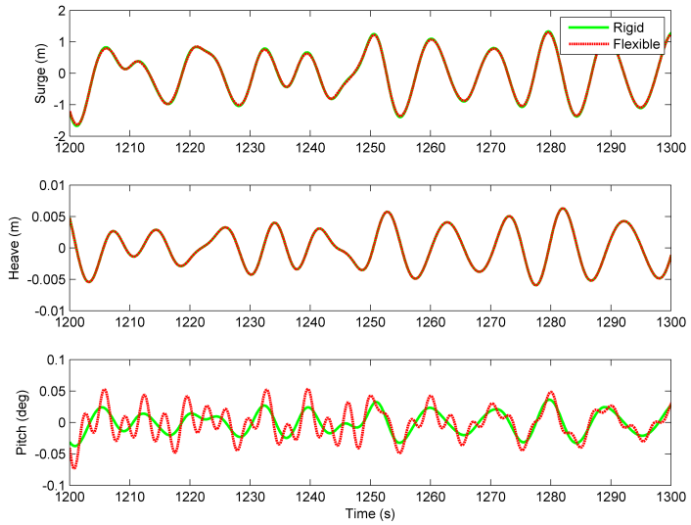

Fig. 19: Effects of tower's flexibility on TLP motions.

DISCUSSION

Simplifications

The main simplifications of the modeling followed in this study are:

- TLP dynamics are heavily simplified by using a spring to model all tendons. The effect of the flexibility of the tendons is totally ignored in this way. Obviously, slack tendon events cannot be modeled. The set-down effect, which is the coupling between heave and surge due to the mooring system, is not modeled here.
- The environment consists of one sea-state of long-crested waves with 0 degree heading. This wave direction enables us

to focus on the surge, heave, pitch, and the first tower fore-aft bending mode and to ignore the sway, roll, and yaw.

- As the pitch eigenfrequency is higher than the wave cut-off frequency for the considered load cases, only the high-frequency component of the second-order wave loads can excite this mode at its resonance frequency.
- Although the wave excitation is calculated up to the second-order, the wave description is still seen as linear. Responses related to nonlinearity in the waves (other than the second-order velocity potential of component V of the QTFs) are not within the scope of this study (i.e. the effect of steep or breaking waves were not examined).
- The viscous damping is modeled as a set of linear damping coefficients for each rigid-body mode. Only the coefficient in surge is determined from the results of a surge-decay model test. The same coefficients are used for the fully rigid TLP and the TLP with the flexible tower. As the viscous damping coefficients in heave and pitch could not be determined from the decay tests with enough accuracy, they were arbitrarily chosen.
- The aerodynamic damping and other turbine operational effects were omitted.

Based on the recommendations of recent research work at NREL (Matha, 2009 and Roald et al, 2013), the main targets of this work were:

- The modeling of the TLP in (WAMIT+FAST) with the recently available second-order loads and its comparison with a similar combination of tools (DIFFRAC+aNySIM).
- The effect of the flexibility of the tower on the simulation results of FAST. Only the lowest structural mode of the tower was considered (first bending mode) because this mode combines with the pitch rigid-body mode of the TLP at a low frequency.

Rigid TLP

All results of this comparison study show that the motion response of the TLP is mainly linear, with the exception of surge. This finding was expected as the mooring system is modeled with a spring matrix, the second-order excitation is much smaller than the first-order wave loads, and the natural frequencies are outside the wave-excitation range. In surge, the second-order difference-frequency excitation occurs in a frequency range that includes the eigenfrequency. Consequently, the effects of the surge difference-frequency loads can still be seen, even if they are small, due to resonance. Figure 20 shows the PSDs of all the distinct wave load contributions: first-order, second-order sum frequency, and second-order difference frequency. The eigenfrequency of each rigid-body mode is marked with a line ending with upward triangles on the same figure. According to this figure, the surge and pitch eigenmodes could be excited by the second-order loads. No significant loading is applied at very high frequencies where the heave eigenfrequency lies. At the surge eigenfrequency, the second-order difference-frequency load is bigger than the first-order loads. As there is no potential damping in surge for very low frequencies, the second-order difference-frequency loads result in a small but noticeable effect on the surge motion (Fig. 18). Note that the choice of the cut-off frequency of the wave spectrum induces the domination of the sum-frequency second-order wave loads over the first-order wave loads above 1.57 (rad/s). The pitch eigenfrequency is close to the upper frequency limit where the sum-frequency second-order loads are still acting. At this frequency, the potential damping in pitch is also nonexistent. Nevertheless, the amplitude of these second-order loads is too small to lead to a remarkable pitch response for the fully rigid TLP (Fig. 18).

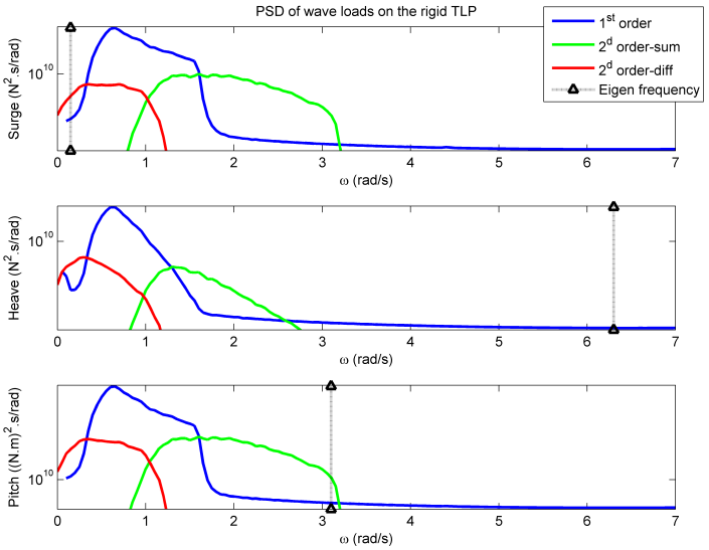

Fig. 20: PSDs of all first- and second-order contributions to the wave loads for the fully rigid TLP

TLP with Flexible Tower

Figure 21 contains the PSDs of the wave loads contributions for the TLP with the flexible tower. Despite of the fact that the second-order loads have been calculated again for the flexible TLP, the PSD of the flexible TLP and the rigid TLP look very similar for all modes (on a log scale at least). The excitation PSDs are plotted together with the eigenfrequencies for the surge mode, the heave mode, and the pitch/first-tower bending mode. As explained before, only the pitch eigenfrequency changes when the tower is modeled as a flexible body. The eigenfrequency in pitch is now in the middle of the pitch sum-frequency excitation range. In this frequency range, the second-order, sum-frequency loads dominate largely all the other contributions, and the amplitudes are close to their maximum value, which is very different from the rigid case in Fig. 20. Logically, an increase of the pitch response can be expected.

PSDs of the motions resulting from FAST simulations with and without the flexible tower are compared in Figs. 22, 23, 24, and 25. The surge motion of the TLP with a flexible tower is largely unchanged compared to those of the fully rigid TLP when second-order wave loads are applied (Fig. 23) or not applied (Fig. 22). The heave is also the same as seen in Fig. 19 (heave-PSDs are not shown). The resonance peak at the surge eigenfrequency is excited when second-order forces are applied (LC2.2-ALL) and is of similar magnitude for the rigid and flexible systems (Fig. 23). Under linear wave excitation exclusively (LC2.2-F1), the pitch-PSDs of both TLPs are very similar (Fig. 24). They show a single peak that corresponds to the (linear) wave excitation response peak. The biggest change occurs in the response to LC2.2-ALL, where the second-order loads are active (Fig. 25). The PSD of the flexible TLP contains a second peak at 1.8 (rad/s), the pitch eigenfrequency, whereas only the first peak of the (linear) wave excitation is present for the rigid TLP. The tower's flexibility shifts the pitch natural frequency such that pitch is now easily excited by second-order wave forces.

Only the pitch eigenfrequency changes when the tower is modeled as a flexible body. This is due to the coupling of the tower's first bending mode and the pitch eigenfrequency of the floater. This shift towards a lower frequency may increase the exposure to first- and second-order wave loads. For the considered TLP, the values of the sum-frequency QTF at the pitch eigenfrequency for the flexible tower (1.8 rad/s) are not significantly higher than those of the sum-frequency at the pitch

eigenfrequency for the fully rigid TLP (3.1 rad/s). This is confirmed by the fact that the PSDs of the second-order sum-frequency loads look the same in Figs. 20 and 21. On the other hand, the wave energy of LC2.2 is concentrated around the peak at 0.63 (rad/s), which leads to a significantly greater amount of energy for sum-frequencies close to 1.8 (rad/s) than for 3.1 (rad/s). As a consequence, the second-order sum-frequency pitch moment is significantly bigger for the TLP with the flexible tower than for the rigid TLP. This greater exposure to the second-order sum-frequency loads at the pitch eigenfrequency causes a pitch response. It should be noted that this amplification of the response to second-order loads is true for the sharp wave energy spectrum of LC2.2, which contains no wave energy above 1.57 (rad/s). In this case, the resonance solely amplifies the response to second-order loads. In a sea-state with a higher cut-off frequency and a shorter wave period and a larger energy spread, the first-order pitch excitation may mask the sum-frequency second-order loads.

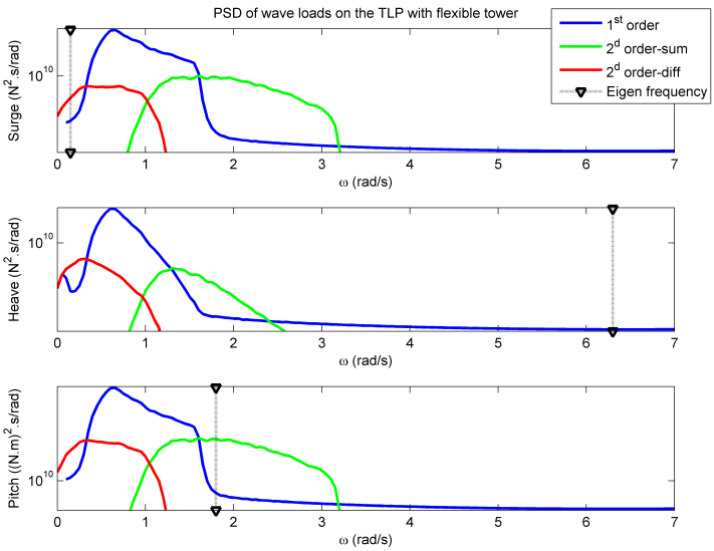

Fig. 21: PSDs of all first- and second-order contributions to the wave loads for the TLP with the flexible tower

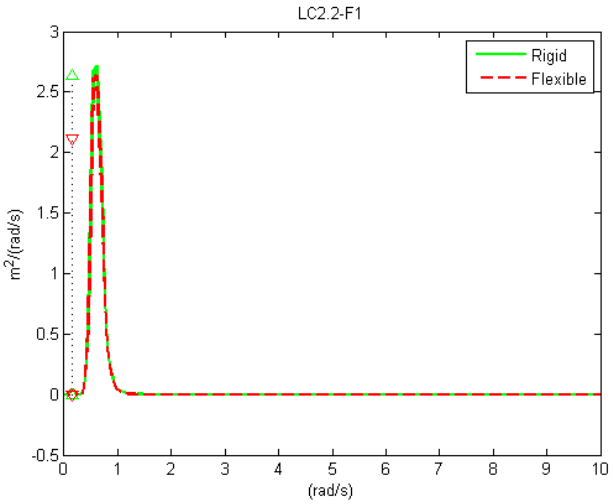

Fig. 22: Effect of tower's flexibility on the surge responses (PSD) for the load case with only first-order wave excitation (LC2.2-F1)

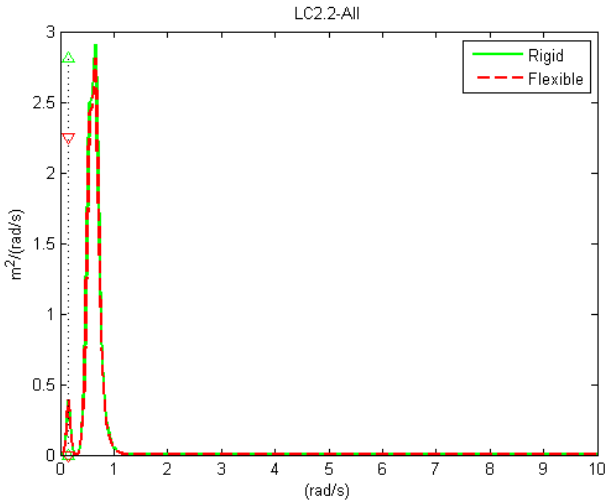

Fig. 23: Effect of tower's flexibility on the surge responses (PSD) for simulations with first- and second-order wave loads (LC2.2-ALL)

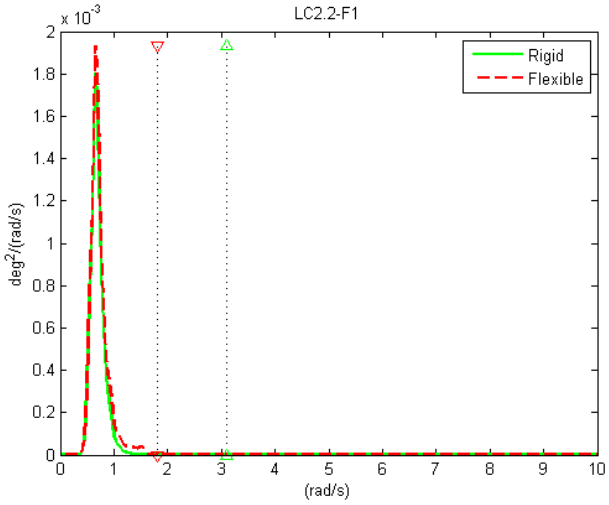

Fig. 24: Effect of tower's flexibility on the pitch responses (PSD) for simulations with first-order wave excitation (LC2.2-F1)

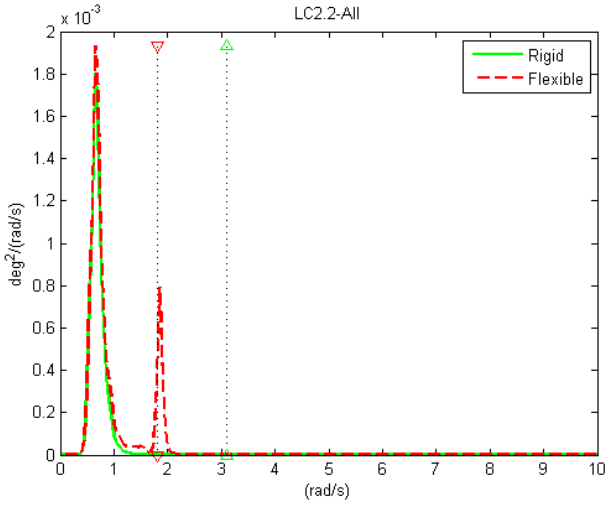

Fig. 25: Effect of tower's flexibility on the pitch responses (PSD) for simulations with first- and second-order wave loads (LC2.2-ALL)

CONCLUSIONS

Two numerical packages (DIFFRAC+aNySIM) and (WAMIT+FAST) were compared using a TLP platform supporting a wind turbine. This comparison was done with the assumption that the TLP is a fully rigid body. The results of both packages in long-crested head waves are very close to each other. It appeared that the TLP, seen as a fully rigid body, had little sensitivity to second-order loads. Indeed, only a small effect on the surge motion could be seen.

A work-around was proposed and applied in this study to include the flexibility of the tower in the calculation of the second-order QTFs. In this approach, the stiffness in pitch was adjusted during the second-order potential-flow calculation to better reproduce the pitch response of the TLP with a flexible tower. As a consequence of this adjustment, a resonance peak appeared in the pitch response. The comparison of the motion results of the TLP with the flexible tower against those of the fully rigid TLP showed a significant increase of the pitch response. This increase is mainly a consequence of the shift of the pitch eigenfrequency for the TLP with the flexible tower to a lower value where the sum-frequency loads are almost at their maximum. These simulations demonstrate that the flexibility of the tower of the turbine can have a major effect on the pitch motion of the TLP. To conclude, the tower's flexibility must be taken into account in the simulations of the TLP in extreme sea-states. Second-order, high-frequency wave loads can trigger a resonance response of the pitch/tower first bending mode of the TLP. This resonance behavior can be reproduced by numerical tools based on potential flow if they include the second-order sum-frequency wave excitation. However, it should also be kept in mind that first-order wave loads can also trigger a resonance response of the pitch/tower first bending mode when this eigenfrequency is not high enough. In such a case, the effects of first-order wave loads would most likely mask those of the second-order sum-frequency loads, which are smaller by nature.

ACKNOWLEDGEMENTS

The authors are obliged to the DeepCwind consortium led by the University of Maine. The work of Tim Bunnik of MARIN is acknowledged for facilitating the addition of the second-order sum frequency loads in the aNySIM's simulations.

REFERENCES

aNySIM User Guide, MARIN, Wageningen, 2009, https://wiki.marin.nl/index.php/ANYwiki

Bunnik, T., 2012, DIFFRAC version 2.4 User Guide, MARIN, Wageningen.

Goupee, A.J., Koo, B.J., Lambrakos, K.F. and Kimball, R.W., 2012, "Model Tests for Three Floating Wind Turbine Concepts," Proc. 2012 Offshore Technology Conference, Houston, Texas.

Gueydon, S., Duarte, T., Jonkman, J., 2014. "Comparison of Second-Order Loads on a Semisubmersible Floating Wind Turbine," 33rd International Conference on Ocean, Offshore and Arctic Engineering (OMAE), San Francisco.

Jonkman, J. and Buhl, Jr., M.L., 2005, FAST User's Guide, Tech. Rep. NREL/EL-500-38230, National Renewable Energy Laboratory.

Jonkman, J., Larsen, T., Hansen, A., Nygaard, T., Maus, K., Karimirad, M., Goa, Z., Moan, T., Fylling, I., Nichols, J., Kohlmeier, M., Vergara, J.P., Merino, D., Shi, W., and Park, H., 2010. "Offshore Code Comparison Collaboration Within IEA Wind Task 23: Phase IV Results Regarding Floating Wind Turbine Modelling," Tech. Rep. NREL/CP-500-47535, National Renewable Energy Laboratory.

Lee, C.H., and Newman, J. N., 2013, WAMIT – User manual version 7.0, WAMIT Inc, Chestnut Hill, Massachusetts.

Matha, D., 2009, "Model Development and Loads Analysis of an Offshore Wind Turbine on a Tension-Leg Platform, with Comparison to Other Floating wind Turbine Concepts". Master's thesis, University of Colorado-Boulder.

Molin, B., Remy, F., and Facon, G., 2004, "Etude experimental du comportment hydro-aero-élastique d'une éolienne offshore sur ancrage tendus," Ocean Energy Conference, Brest, France.

Pinkster, J. A., 1980, "Low Frequency Second Order Wave Exciting Forces on Floating Structures," NSMB Publication No. 650, Wageningen, Netherlands.

Prowell, I., Robertson, A., Jonkman, J., Stewart, G., and Goupee, A, "Numerical Prediction of Experimentally Observed Scale-Model Behavior of an Offshore Wind Turbine Supported by a Tension-Leg Platform," Proc. 2013 Offshore Technology Conference, Houston, Texas.

Roald, L., Jonkman, J., Robertson, A., Chokani, N., 2013, "The Effect of Second-order Hydrodynamics on Floating Offshore Wind Turbine," NREL, Golden, Colorado.

Robertson, A., Jonkman, J., Masciola, M., Song, H., Goupee, A., Coulling, A., Luan, C., 2012, "Definition of Semisubmersible Floating System for Phase II of OC4," Technical Report NREL/TLP-5000-60601.

Robertson, A., Fabien, V. and OC4-participants , 2014, "Offshore Code Comparison Collaboration Continuation Within IEA Task 30: Phase II Results Regarding A Floating Semisubmersible Wind System," 33rd International Conference on Ocean, Offshore and Arctic Engineering (OMAE), San Francisco.

Wuillaume, P. Y., 2014, "Comparison of DIFFRAC, WAMIT, aNySIM and FAST," Internship's report, Ecole Centrale de Nantes.